ISSN: 2414-1895 DOI: 10.6919/ICJE.202505_11(5).0047

Solid State-Hydrothermal Synthesis and Photoluminescence of ZnS

Hai Li*

School of Physics and Optoeletronic Engineering, Guangdong university of technology, Guangzhou, Guangdong, 510006, China

Abstract

This study reports a novel solid-state-hydrothermal hybrid strategy for synthesizing phase-pure cubic ZnS. Starting with the high-temperature solid-state synthesis of K2Zn3S4 precursor, subsequent hydrothermal deintercalation yielded ZnS powders with cubic zinc-blende structure. Optical characterization revealed a direct bandgap of 3.50 eV and prominent red emission at 620 nm (2.0 eV) under 365 nm excitation, which can be attributed to de-trapping recombination between sulfur vacancies and zinc vacancies. This work establishes a dopant-free pathway for engineering ZnS luminescence through intrinsic defect control.

Keywords

Zinc Sulfide; Vacancy Defect; Photoluminescence Spectroscopy.

1. Introduction

Phosphors, as one of the critical classes of luminescent materials, play a pivotal role in modern optoelectronic technology. They are widely used in lighting, display devices, biological imaging, and sensors due to their efficient photoluminescence properties[1, 2]. Their fundamental working principle involves absorbing energy at specific wavelengths and subsequently re-emitting photons at different wavelengths, thereby achieving energy conversion and photon re-emission[3]. Common phosphor materials include oxides, sulfides, and nitrides[4, 5].

Among the various phosphor materials, ZnS has become a research hotspot due to its direct bandgap properties and tunable optical characteristics[6-8]. ZnS is a typical II-VI semiconductor with a direct bandgap structure, possessing a bandgap energy of approximately 3.6-3.8 eV[9]. This wide bandgap allows ZnS to exhibit strong absorption in the ultraviolet region and excellent luminescence performance in the visible light range. By doping ZnS with different activators, such as copper (Cu) or manganese (Mn), multicolor emissions in the visible light range can be achieved[10-12]. For instance, The luminescence mechanism in Cu-doped ZnS predominantly arises from donor-acceptor trap-assisted electron-hole recombination processes[13].

Various synthesis methods have been developed for ZnS-based phosphors, including mechanical ball milling[14, 15], low eutectic flux methods, and ultrasonic techniques[16-18]. These methods enable the tuning of ZnS luminescence properties by altering the microstructure of material and the distribution of activators. Research has shown that fabrication techniques significantly influence phosphor performance, and uniform distribution of activators within the ZnS matrix is critical for enhancing luminescence efficiency[19, 20].

In recent years, nanostructured ZnS phosphors have attracted extensive interest due to their unique optical properties and potential applications[21, 22]. Particularly, the synthesis methods and luminescent properties of Mn-doped ZnS nanophosphors have been intensively investigated, demonstrating promising applications in biological labeling and display technologies[23]. The

ISSN: 2414-1895 DOI: 10.6919/ICJE.202505_11(5).0047

luminescent performance of ZnS-based phosphors is also influenced by factors such as crystal structure, particle size, and surface defects[24-26]. By optimizing fabrication processes and doping strategies, precise control over ZnS luminescence characteristics can be achieved[27]. This defect engineering strategy has been successfully implemented in optical anti-counterfeiting systems, where ZnS-based tags exhibit excitation-dependent chromaticity shifts responsive to UV/IR stimulation[28].

Despite these advancements, the intrinsic photophysics of undoped ZnS remain insufficiently explored. In-depth investigations into the luminescence mechanisms and fabrication processes of ZnS are essential for developing high-performance luminescent materials. In this study, cubic-phase ZnS was synthesized via a sequential approach: $K_2Zn_3S_4$ was first prepared by high-temperature solid-state reaction, followed by hydrothermal deintercalation to obtain the phase-pure cubic ZnS. The resulting material exhibits red emission at 620 nm under UV excitation. These findings provide valuable insights into the structural and optical properties of ZnS, laying a foundation for its application in optoelectronic devices such as LEDs and displays.

2. Experimental

2.1 Synthesis

The cubic-phase ZnS was prepared through a hybrid approach involving solid-state synthesis followed by hydrothermal treatment. The zinc powder (99.99%, Aladdin) and sulfur powder (99.5%, Alfa Aesar) were mixed in a molar ratio of 3:4, thoroughly ground and homogenized in an agate mortar. The mixture was pressed to pellets, accurately weighed, and transferred into a high-purity alumina crucible. The required amount of potassium metal S (99.5%, Alfa Aesar) was calculated based on the stoichiometric requirements and added to the crucible. The reaction system was sealed using vacuum-sealed quartz tube encapsulation technology. The encapsulated sample was placed in a muffle furnace, heated gradually to 1020 °C, and annealed for 60 h before cooling to room temperature, ultimately yielding $K_2Zn_3S_4$ single crystals. For the hydrothermal reaction, 0.1 g of sodium hydroxide and 0.4 g of thiourea were added to a 25 mL telfon liner containing 5 mL of deionized water. After allowing the solution to stand until complete dissolution of the reagents, the as-synthesized K2Zn3S4 crystals were transferred to the PTFE liner, ensuring full immersion in the reaction solution. The liner was tightly sealed within a stainless-steel autoclave and subjected to hydrothermal treatment at 120 °C for 12 h. After cooling to room temperature, the autoclave was opened, and the precipitate was collected. The final product was washed repeatedly with deionized water and vacuum-dried at room temperature.

2.2 Characterization

Powder X-ray diffraction (PXRD) data were collected on a Bruker D8 Focus X-ray diffractometer using Cu Kα radiation. The morphology and composition of the ZnS samples were analyzed using a Regulus 8100 scanning electron microscope (SEM) and an energy-dispersive X-ray spectroscopy (EDS) instrument manufactured by Hitachi in Japan. The photoluminescence excitation (PLE) and emission (PL) spectra, and time-gated photoluminescence decay curves of the ZnS samples were acquired using a Fluorescence Spectrophotometer Fluorolog-3 instrument manufactured by HORIBA Instruments Incorporated, USA. UV-Vis-NIR absorption spectra were acquired using a SHIMADZU UV-3600 Plus spectrophotometer in diffuse reflectance mode with $BaSO_4$ as reference standard.

3. Results and Discussion

3.1 Morphology and Structure Analysis

Fig. 1 shows the XRD pattern of ZnS synthesized via hydrothermal deintercalation. The peaks of the prepared ZnS sample prepared were confirmed to coincide with the F-43m space group of cubic phase ZnS, where four diffraction peaks at 28.56°, 33.09°, 47.52°, and 56.29°which correspond to the (1 1 1), (0 0 2), (2 2 0), and (3 1 1) plane (JCPDS cards No. 05-0566, a = 5.406 Å). The diffraction peaks of all the samples match the positions of the standard card.

ISSN: 2414-1895 DOI: 10.6919/ICJE.202505_11(5).0047

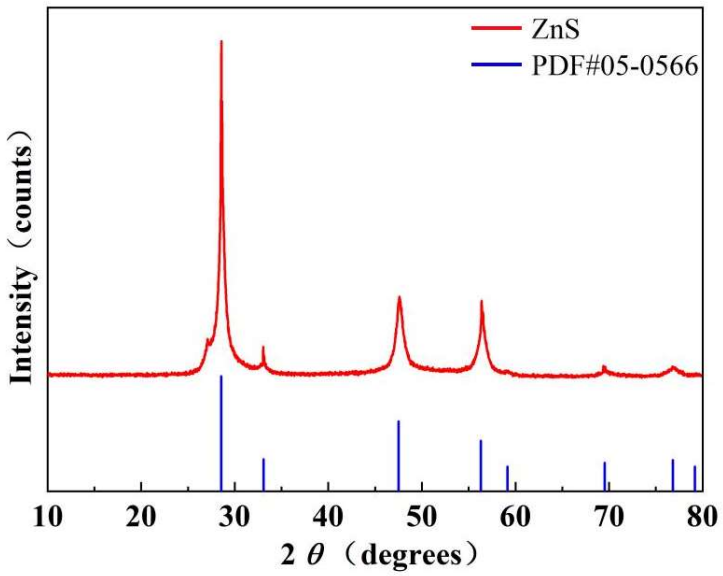

Fig. 1 XRD patterns of ZnS synthesized via hydrothermal deintercalation.

As shown in Fig. 2, the SEM images of ZnS synthesized via hydrothermal deintercalation. The surface morphology and microstructure of the samples were systematically characterized using scanning electron microscopy (SEM), coupled with energy-dispersive X-ray spectroscopy (EDS) for quantitative elemental analysis. The ZnS powder synthesized via chemical deintercalation exhibits an irregular polyhedral morphology under SEM observation, with crystal dimensions reaching up to 10 μm. EDS elemental mapping confirms homogeneous distribution of zinc and sulfur throughout the sample, with no detectable elemental segregation or localized enrichment. Quantitative EDS measurements (Table 1) reveal a near-stoichiometric Zn and S atomic ratio of approximately 1:1, consistent with the ideal composition of ZnS.

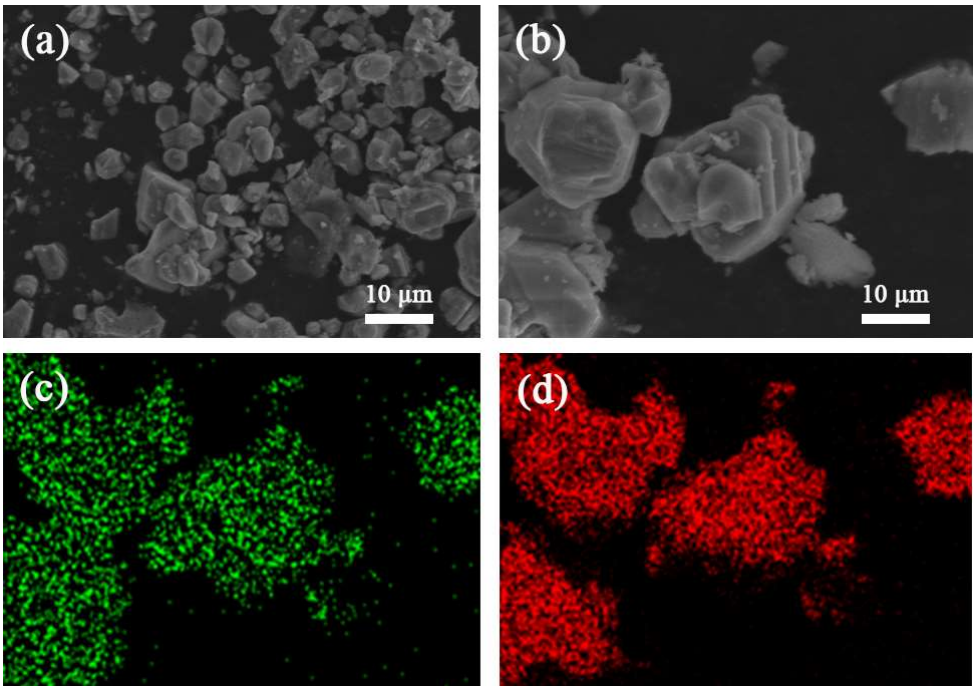

Fig. 2 SEM images and EDS-element mapping of ZnS synthesized via hydrothermal deintercalation.

ISSN: 2414-1895 DOI: 10.6919/ICJE.202505_11(5).0047

Table 1. Atomic percent of the ZnS sample and the Zn/S ratio

Sample	EDS (atomic%)		
	Zinc	Sulphur	Zn/S
ZnS	50.009	49.991	1

3.2 The Optical Characteristics

Fig. 3 shows the UV–vis absorption characteristics of the prepared ZnS synthesized via hydrothermal deintercalation. The characteristic absorption peak of the ZnS particle appears in the wavelength range of 320– 400 nm, and the peak position reflects the band gap of the particles. Corresponding to the fundamental absorption of the electrons from the valence band excitation to the conduction band, it can be used to determine the properties and values of the optical bandgap of the prepared ZnS. In order to obtain absorption characteristics for all samples, the transmittance (T) was first measured at different wavelengths (λ), and then the absorption coefficient (α) at the corresponding wavelength λ was calculated using the Beer–Lambert's relation[29] (Eq. (1)).

$$\alpha = \frac{1}{\mathrm{d}} \ln\left(\frac{1}{T}\right) \tag{1}$$

Where d is the path length. The following relation gives the relationship between the incident photon energy (hν) and the absorption coefficient (α) (Eq. (2)).

$$(\alpha h\upsilon)^{1/m} = c(h\nu - E_g) \tag{2}$$

Where the exponential m depends on the type of transition and c is a constant and Eg is the band gap of the material. For the direct transition $m = \frac{1}{2}$, direct forbidden transition $m = \frac{3}{2}$, and for the indirect transition m = 2. The optical band gap was determined using Tauc plot methodology for direct bandgap semiconductors. by plotting the diagram $(\alpha h\nu)^2$versus hν, and then extrapolating its linear portion of its intersection with the horizontal axis, the hν value corresponding to the intersection is the optical band gap of the material. Fig. 4 shows that the band gaps for ZnS is 3.50 eV.

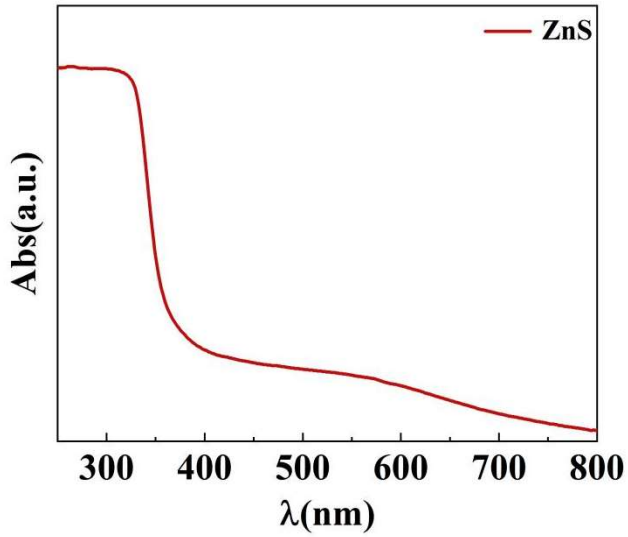

Fig. 3 UV–vis absorption characteristics of the prepared ZnS.

ISSN: 2414-1895 DOI: 10.6919/ICJE.202505_11(5).0047

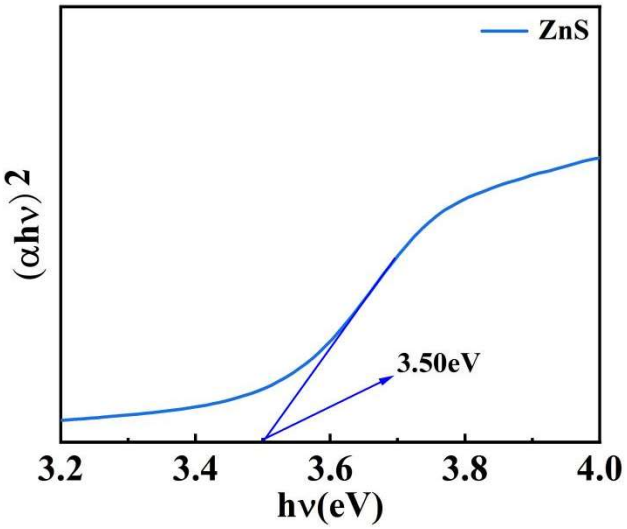

Fig. 4 The optical band gap was calculated by UV-visible absorption/transmission spectroscopy.

It is generally believed that there were four types of point defects (schematically shown in Fig. 5) in ZnS that serve as the main luminescent sites: sulfur vacancies (V_s), interstitial sulfur (I_s), zinc vacancies (V_{Zn}), and interstitial zinc (I_{Zn})[30]. These defects can be classified into two categories based on their unique electronic properties and energy levels. Sulfur vacancies and interstitial zinc atoms are equivalent localized donor states, while zinc vacancies and interstitial sulfur atoms are equivalent acceptor states[31], Denzler et al[32]. reported that the interstitial sulfur states should be closer to the valence band edge than the interstitial zinc states, while the sulfur vacancies should be closer to the conduction band edge than the zinc vacancies. Moreover, the energy levels of the vacancies are deeper than the energy levels of the interstitial states. Specific defects were identified by performing photoluminescence testing. Fig. 6 shows the excitation and emission spectra of ZnS synthesized via hydrothermal deintercalation. The ZnS sample photoluminescence spectrum at 365 nm shows emission peaks at 620 nm. The red emission at 620 nm was attributed to the de-trap recombination process between sulfur vacancies and zinc vacancies[30, 31]. In the ZnS sample, the energy level difference between sulfur vacancies (V_s) and zinc vacancies (V_{Zn}) is small, and the electrons are localized between these defect centers. When the ZnS sample is excited, the electrons are captured from the sulfur vacancy (V_s), and after the localization process, they may jump to the zinc vacancy (V_{Zn}), eventually recombined between the two defects, leading to red light emission.

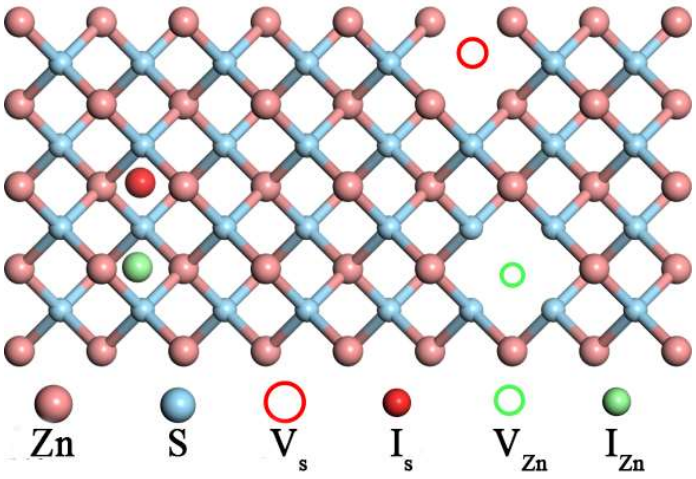

Fig. 5 Schematic representation of possible point defects in pure ZnS.

ISSN: 2414-1895 DOI: 10.6919/ICJE.202505_11(5).0047

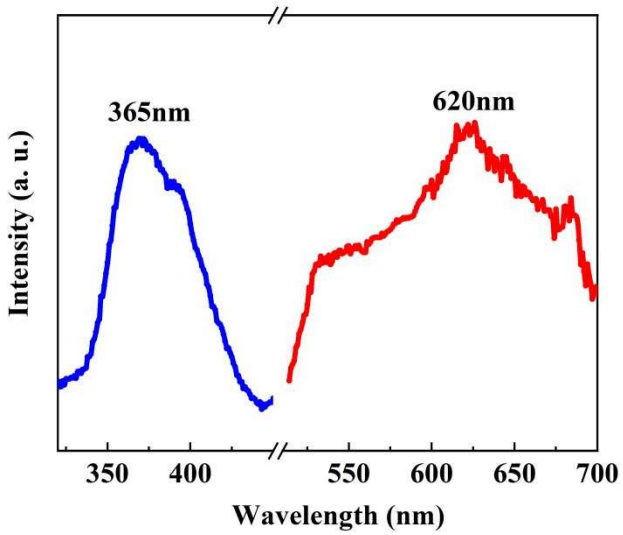

Fig. 6 The excitation and emission spectra of ZnS samples.

The decay behavior of the ZnS samples were tested at 320 nm excitation as shown in Fig.7. The curve can be well fitted by the second-order exponential decay formula[33] (Eq. (3))

$$I = A_1 \exp(-t/\tau_1) + A_2 \exp(-t/\tau_2) \tag{3}$$

Where I is the luminescence intensity, A1 and A2 denote amplitude coefficients, t is the time, and τ_1 and τ_2 represent characteristic lifetimes associated with distinct radiative decay channels. The average fluorescence lifetime of the ZnS can be calculated 3.82 ns.

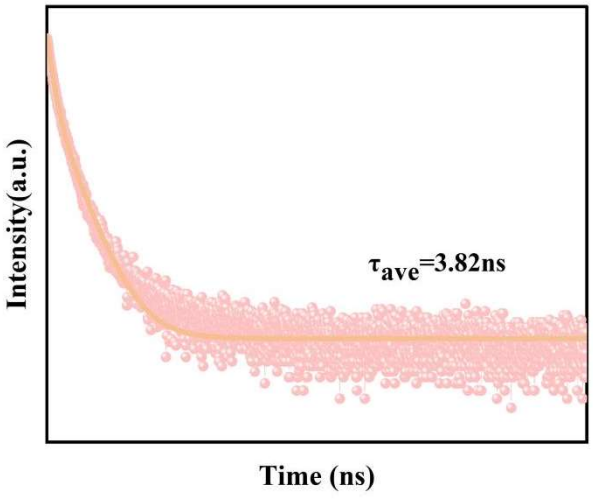

Fig. 7 Decay curves of ZnS synthesized via hydrothermal deintercalation.

4. Conclusion

This work establishes a dopant-free strategy for engineering the luminescent properties of cubic ZnS through controlled defect generation, achieved via a novel solid-state precursor-hydrothermal deintercalation synthesis route. By precisely regulating the deintercalation kinetics of $K_2Zn_3S_4$, phase-pure ZnS with zinc blende structure and near-stoichiometric composition (Zn:S ≈1:1) was successfully synthesized, as validated by XRD and EDS mapping. The material exhibits distinctive red emission at 620 nm under UV excitation, attributed to detrapping recombination between sulfur

ISSN: 2414-1895 DOI: 10.6919/ICJE.202505_11(5).0047

vacancies and zinc vacancies, with a fluorescence lifetime of 3.82 ns confirming defect-mediated carrier dynamics. These findings provide an alternative way to engineer the luminescence properties of ZnS.

Acknowledgments

This work was financially supported by the National Natural Science Foundation of China (Grant Nos. 51702058).

References

[1] Xing X, Cao W W, Wu Z X, et al. Microstructural and luminescence characteristics of high-linearity ZnS:Cu2+,Cl- phosphor [J]. Journal of Materials Science-Materials in Electronics, 2023, 34(5).

[2] Heiba Z K, Albassam A A, Mohamed M B. Effect of Zn/S non-stoichiometric ratio on the structural, optical and electronic properties of nano-ZnS [J]. Applied Physics A, 2020, 126(6): 479.

[3] Zhang C, Zhu X Z. n-Type Quinoidal Oligothiophene-Based Semiconductors for Thin-Film Transistors and Thermoelectrics [J]. Advanced Functional Materials, 2020, 30(31).

[4] Suresh L, Bondili J S, Brahman P K. Development of proof of concept for prostate cancer detection: an electrochemical immunosensor based on fullerene-C60 and copper nanoparticles composite film as diagnostic tool [J]. Materials Today Chemistry, 2020, 16.

[5] Wu R R, Wang C J, Dibble T S. First experimental kinetic study of the atmospherically important reaction of BrHg + NO2 (vol 759, 137928, 2020) [J]. Chemical Physics Letters, 2022, 787.

[6] Cui J Y, Zeng X H, Zhou M, et al. Tunable blue and orange emissions of ZnS:Mn thin films deposited on GaN substrates by pulsed laser deposition [J]. Journal of Luminescence, 2014, 147: 310-5.

[7] Lu J L, Zhang X Q, Liu D D, et al. Review of Dielectric Carbide, Oxide, and Sulfide Nanostructures for Electromagnetic Wave Absorption [J]. Acs Applied Nano Materials, 2023, 6(17): 15347-66.

[8] Curcio A L, da Silva L F, Bernardi M I B, et al. Nanostructured ZnS:Cu phosphor: Correlation between photoluminescence properties and local structure [J]. Journal of Luminescence, 2019, 206: 292-7.

[9] Hao X Q, Wang Y C, Zhou J, et al. Zinc vacancy-promoted photocatalytic activity and photostability of ZnS for efficient visible-light-driven hydrogen evolution [J]. Applied Catalysis B-Environmental, 2018, 221: 302-11.

[10] Yang P, Lü M, Xü D, et al. Synthesis and photoluminescence characteristics of doped ZnS nanoparticles [J]. Applied Physics A, 2001, 73(4): 455-8.

[11] Ummartyotin S, Bunnak N, Juntaro J, et al. Synthesis and luminescence properties of ZnS and metal (Mn, Cu)-doped-ZnS ceramic powder [J]. Solid State Sciences, 2012, 14(3): 299-304.

[12] Sundhar A. Development of ZnS thin film with Co, Cu and Ag doping using SILAR method; proceedings of the International Conference on Impact of Innovations in Science and Technology for Societal Development (IISTSD) - Materials Science, India, F Sep 19-21, 2019 [C]. 2022.

[13] Rastogi C K, Mishra R K, Chirauri S, et al. Comparative study on photo and electroluminescence properties of Cu-doped ZnS [J]. Physica B-Condensed Matter, 2022, 640.

[14] Pathak C S, Mandal M K, Agarwala V. Synthesis and characterization of zinc sulphide nanoparticles prepared by mechanochemical route [J]. Superlattices and Microstructures, 2013, 58: 135-43.

[15] Pathak C S, Mishra D D, Agarwala V, et al. Optical properties of ZnS nanoparticles produced by mechanochemical method [J]. Ceramics International, 2012, 38(8): 6191-5.

[16] Cadis A I, Perhaita I, Munteanu V, et al. Influence of preparative conditions for obtaining ZnS:Mn nanoparticles using ultrasound-assisted precipitation [J]. Colloid and Polymer Science, 2017, 295(12): 2337-49.

[17] Tang Y L, Tian J L, Malkoske T, et al. Facile ultrasonic synthesis of novel zinc sulfide/carbon nanotube coaxial nanocables for enhanced photodegradation of methyl orange [J]. Journal of Materials Science, 2017, 52(3): 1581-9.

[18] Bach L G, Islam M R, Binh M T, et al. Ultrasound-Assisted Synthesis of Hybrid Nanostructures Using RAFT Polymerization from the Surface of Quantum Dots [J]. International Journal of Precision Engineering and Manufacturing, 2013, 14(6): 937-42.

ISSN: 2414-1895 DOI: 10.6919/ICJE.202505_11(5).0047

[19] Sychov M M, Ogurtsov K A, Lebedev V T, et al. Effect of the Cu content and ZnS treatment on the characteristics of synthesized ZnS:(Cu, Cl) electroluminescent phosphors [J]. Semiconductors, 2012, 46(5): 696-700.

[20] Wang W D, Huang F Q, Xia Y J, et al. Effect of activator distribution on photo- and X-ray excited luminescence properties of ZnS:Cu,Cl phosphors [J]. Materials Research Bulletin, 2008, 43(7): 1892-7.

[21] Dai L W, Lesyuk R, Karpulevich A, et al. From Wurtzite Nanoplatelets to Zinc Blende Nanorods: Simultaneous Control of Shape and Phase in Ultrathin ZnS Nanocrystals [J]. Journal of Physical Chemistry Letters, 2019, 10(14): 3828-35.

[22] Dai L, Strelow C, Kipp T, et al. Colloidal manganese doped ZnS nanoplatelets and their optical properties [J]. Arxiv, 2021.

[23] Dong B H, Cao L X, Su G, et al. Synthesis and characterization of Mn doped ZnS d-dots with controllable dual-color emissions [J]. Journal of Colloid and Interface Science, 2012, 367: 178-82.

[24] Raleaooa P V, Roodt A, Mhlongo G G, et al. Analysis of the structure, particle morphology and photoluminescent properties of ZnS:Mn2+ nanoparticulate phosphors [J]. Optik, 2018, 153: 31-42.

[25] Wright A C, Viney I V F. A structural evaluation of ZnS-based electroluminescent phosphors and devices: a comparison with performance [J]. Philosophical Magazine B-Physics of Condensed Matter Statistical Mechanics Electronic Optical and Magnetic Properties, 2001, 81(3): 279-97.

[26] Ibafiez J, Garcia E, Gil L, et al. Frequency-dependent light emission and extinction of electrolumine scent ZnS:Cu phosphor [J]. Displays, 2007, 28(3): 112-7.

[27] Demirselcuk B, Kus E, Kucukarslan A, et al. Optimization of chemically sprayed ZnS films by Mn doping [J]. Physica B-Condensed Matter, 2021, 622.

[28] Wei Z R, Lu Y, Zhao J, et al. Synthesis and Luminescent Modulation of ZnS Crystallite by a Hydrothermal Method [J]. Acs Omega, 2018, 3(1): 137-43.

[29] Sarkar R, Tiwary C S, Kumbhakar P, et al. Yellow-orange light emission from Mn2+-doped ZnS nanoparticles [J]. Physica E-Low-Dimensional Systems & Nanostructures, 2008, 40(10): 3115-20.

[30] Zhou J, Zhao J, Liu R. Defect engineering of zeolite imidazole framework derived ZnS nanosheets towards enhanced visible light driven photocatalytic hydrogen production [J]. Applied Catalysis B-Environmental, 2020, 278.

[31] Wang X L, Shi J Y, Feng Z C, et al. Visible emission characteristics from different defects of ZnS nanocrystals [J]. Physical Chemistry Chemical Physics, 2011, 13(10): 4715-23.

[32] Denzler D, Olschewski M, Sattler K. Luminescence studies of localized gap states in colloidal ZnS nanocrystals [J]. Journal of Applied Physics, 1998, 84(5): 2841-5.

[33] Lee S Y, Shin Y H, Kim Y, et al. Thermal quenching behavior of emission bands in Eu-doped ZnS nanowires [J]. Journal of Luminescence, 2011, 131(7): 1336-9.